Microchemical Journal, Volume 179, August 2022, Article number 107521
DOI:10.1016/j.microc.2022.107521

Nitrogen-Doped Graphdiyne Quantum-dots as an Optical-Electrochemical Sensor for Sensitive Detection of Dopamine

Qiang Bai[a,1], Hongyang Luo[a,1], Xuetao Yi[b], Shugao Shi[a], Lina Wang[c,*], Manhong Liu[a], Fanglin Du[a], Zhugen Yang[d], Ning Sui[a,*]

[a] College of Materials Science and Engineering, Qingdao University of Science and Technology, Qingdao 266042, China

[b] Qingdao Institute for Food and Drug Control, Qingdao 266000

[c] College of Environment and Safety Engineering, Qingdao University of Science and Technology, Qingdao, 266042, China.

[d] Cranfield Water Science Institute, Cranfield University, Milton Keynes, MK43 0AL, United Kingdom

* Corresponding authors: suining@qust.edu.cn (N. Sui), lnwang2006@163.com (L.N. Wang)

[1] Qiang Bai and Hongyang Luo contributed to this work equally

ABSTRACT: Graphdiyne quantum dots (GDQDs) have attracted increasing attentions due to its unique electronic, optical, and electrochemical properties. However, the low conductivity and quantum yield of GDQDs limit their application. Here, nitrogen-doped graphdiyne dots (N-GDQDs) are firstly synthesized by a simple, friendly and one-step hydrothermal method. The N-GDQDs show a maximum emission at 420 nm under the excitation wavelength of 319 nm. The doping N modifies the surface defect of N-GDQDs and further greatly improves their quantum yield (from 14.6% to 48.6%). In addition, the doping N induces a strong electron transport ability and good conductivity of N-GDQDs. Subsequently, the prepared N-GDQDs are used for constructing an optical-electrochemical nanosensor for sensitive and selective detection of dopamine (DA). DA can quench the fluorescence of N-GDQDs by forming a ground-state non-fluorescent complex between phenoxy anions (in PBS solution) in DA and pyridinic N sites of N-GDQDs, which leads to a highly sensitive and selective detection of DA with a limit of detection (LOD) of 0.14 μM and a linear range of 0.32-500 μM. In the electrochemical detection, DA can be oxidized to DA-benzodiquinone under the electric field through N-GDQDs/GCE, which shows a big affinity to N-GDQDs. The LOD for DA is 0.02 μM with a linear range of 0.05-240 μM. Finally, the real application for DA detection in human serum samples is investigated, the results show that the method has high accuracy. Our work provides a new carbon quantum dots based sensing platform, which shows great potential in practical application.

KEYWORDS: graphdiyne dots, nitrogen-doped, fluorescence, electrochemical, dopamine

Published by Elsevier. This is the Author Accepted Manuscript issued with: Creative Commons Attribution Non-Commercial No Derivatives License (CC:BY:NC:ND 4.0).
The final published version (version of record) is available online at DOI:10.1016/j.microc.2022.107521. Please refer to any applicable publisher terms of use.

1. Introduction

Dopamine (DA) is the most abundant catecholamine neurotransmitter in the brain. It exists in the central nervous system, renal system, cardiovascular system and hormonal system of mammals, and plays an exciting or inhibitory role in physiological activities [1-3]. Higher levels of DA can lead to increasing of heart rate, high blood pressure, heart failure and drug addiction [4]. Lower levels of DA may lead to stress. In addition, low DA levels are also associated with diseases such as Parkinson's disease [5], schizophrenia [6], Alzheimer's disease [7] and depression [8]. Obviously, in order to understand the biological function of DA and its related biological processes and mechanisms, it is necessary to carry out real-time determination of DA in vivo [3].

At present, many classical detection methods have been established for DA, such as fluorescence spectroscopy [9], ultraviolet colorimetric method [10], surface enhanced Raman spectroscopy [11], electrochemical method [12], high performance liquid chromatography (HPLC) [13] and so on. However, these single classical technologies have some shortcomings. For example, electrochemical detection is considered to be an effective detection method because of its simple operation, low cost, fast detection speed, high sensitivity and low detection limit, but its linear range is narrow [14-16]. The fluorescent method has a large detection range, and the process is simple and fast [17, 18], but the sensitivity needs to be further improved [19, 20]. Hence, the combination of fluorescent and electrochemical techniques can make up for the shortcomings of every single method, enabling sensitive and selective detection of DA for a wide range of application.

Graphdiyne (GDY) is a new two-dimensional carbon nanomaterial comprising sp^{2-} and sp^{-}hybridized carbon atoms with high π-conjugation. It has large triangular rings composed of 18 carbon atoms, which form uniformly distributed pores. Graphdiyne quantum dots (GDQDs) are a new type of zero-dimensional luminescent nanomaterials with great development prospects [21]. GDQDs exhibit stable luminescence, excellent biocompatibility and low toxicity, and have a great potential in biomedical sensors, medical imaging, electronics, semiconductors and other fields [21-23]. Nitrogen is a commonly used element doped in carbon-based materials because its atomic size and

valence electrons can bind to carbon atoms [24]. Due to the quantum confinement effect of GDQDs and the presence of sp and sp^2 sites, nitrogen-doped GDQDs may exhibit different optical properties and quantum yield by modulating the band gap, which was reported in N-doped graphene quantum dots (GQDs) [25]. The conductivity and electron transfer rate of GDQDs can be enhanced by doping N element. Because of the high π-conjugation conjugate structure of GDQDs, DA can be adsorbed by π-π stacking, and enhanced DA signal can be obtained due to its excellent electrical properties. Nitrogen can change the electronic structure of GDQDs, and the quantum yield can be enhanced from 14.6% [26] to 48.6%. High quantum yield can improve the detection sensitivity, thus improving the fluorescent property of GDQDs by doping N processes is of great significance.

To the best of our knowledge, this is the first report on N-doped GDQDs (N-GDQDs). Here, N-GDQDs are successfully prepared by hydrothermal method, and the doping N greatly enhances the quantum yield of N-GDQDs. In addition, through the study of the electrochemical properties of N-GDQDs, they have strong electron transport ability and good conductivity. On this basis, we design an optical-electrochemical sensor to detect DA, as shown in the Scheme. 1. A non-fluorescent complex is formed between the N-GDQDs substance and DA to reduce fluorescence; under the action of electric field, DA is oxidized to DA-benzodiquinone by N-GDQDs/GCE to generate a current signal. The optical-electrochemical sensor has high detection sensitivity and a broad detection range. Finally, N-GDQDs are successfully applied to the quantitative determination of DA in human serum. Our work provides a new carbon quantum dot as an optical-electrochemical sensor for DA detection, which shows a good practical application prospect.

<Scheme 1>

2. Experimental

2.1. Materials and Methods

Urea (CH_4N_2O), Dopamine ($C_8H_{11}NO_2$), KCl, NaCl, Glycine, L-cystein, Sodium Nitrate, Hydrogen Peroxide, Glucose, Histamine, Glutamic acid, β-phenethylamine, tyramine and catechol were purchased from Sinopharmaceutical Group Chemical

Reagent Co., Ltd. THF and TBAF were purchased from Aladin Ltd. All reagents and solvents were not further purified after purchase. Ultra-pure water was used throughout the experiment. Electrochemical measurements were carried out on an electrochemical analyzer (CHI660E, CH Instruments, Shanghai Chen Hua Co, China) at room temperature by using a three-electrode system consisting of the glassy carbon electrode as the working electrode, a saturated calomel reference electrode, and a platinum auxiliary electrode. Fluorescent emission (FL) spectra were recorded on a Hitachi F-4700 luminescence spectrometer (Hitachi High-Tech Co., Ltd.). Transmission electron microscopy (TEM) images, high-resolution TEM (HRTEM) images were obtained using JEOL JEM-2100Plus. Fourier transform infrared (FT-IR) spectra were recorded on a Magna-560 spectrometer (Nicolet, Madison, WI). X-ray photoelectron spectroscopy (XPS) was measured on a Thermo ESCALAB VG Science 250 spectrometer with monochromatic Al Kα excitation. The Raman spectra were analyzed by T64000 of HORIBA Scientific Company.

2.2. Materials Synthesis

The preparation of Graphdiyne (GDY) powder has been stated in our previous work [26]. Firstly, the GDY powder (10 mg) was dissolved in ultra-pure water (10 mL) and crushed by ultrasonic (120 W, 30 kHz) for 24 h. The mixture was separated by centrifugation and the liquid was obtained. The obtained is GDQDs. Then, the GDQDs liquid (10mL) was transferred into polytetrafluoroethylene autoclave and heated at 200 ^{o}C for 8 h by adding CH_4N_2O (2.0 mg). Finally, after 24 h of dialysis, the final N-GDQDs was obtained.

2.3. Electrochemical detection of DA

Electrochemical measurements were carried out by using a three-electrode system consisting of the glassy carbon electrode (GCE) as the working electrode, Ag/AgCl electrode as the reference electrode, and a platinum auxiliary electrode. Before the measurement, the bare GCE (3 mm) was cleaned in 0.2 M H_2SO_4 solution, polished with Al_2O_3 powder and cleaned by ultrapure water. The cleaning process was to ensure adequate cleaning of the electrode surface. After it was dried, 6 μL of N-GDQDs solution (0.5 mg mL^{-1}) was dropped on the clean surface of GCE and dried at ambient

condition. Differential pulse voltammetry (DPV) measurements were performed in 0.1 M PBS (pH=7.0). DA as the redox substances with different concentrations were added to the electrolyte. To obtain well-defined oxidation current peaks, the DPV measurements for DA detection were performed in the potential range from -0.6 to 0.2 V. The amplitude, pulse width, and pulse period were set as 50 mV, 0.05 s and 0.25 s.

In the selective test, 0.1 mol L^{-1} PBS (pH = 7.0) solution is used as the buffer solution in the chronoamperometric mode, 50 μmol L^{-1} DA and interfering substances were added to the solution at regular intervals. The concentration of the interfering substances was 1 mmol L^{-1}, the interval was 50 s, and the working voltage was 0.84 V.

2.4. Fluorescence detection of DA

In a typical operation, 100 μL of N-GDQDs (0.1 mg mL^{-1}) solution was added to a PBS buffer solution (0.1 mol L^{-1}, pH = 6.0). 100 μL of DA solution with different concentrations were added to the N-GDQDs solution to form a 1 mL solution. The fluorescence intensity of the system in the presence of DA was detected at 319 nm excitation.

2.5. Application test of DA in actual sample testing

Standard addition method was used to analyze the practicability of DA detection in human serum. In fluorescent detection, N-GDQDs (0.1 mg mL^{-1}) was added to human serum samples containing different concentrations of DA. After 2 min, the fluorescence spectra were recorded at 319 nm excitation wavelength under room temperature. In electrochemical detection, 6 μL N-GDQDs solution (0.1 mg mL^{-1}) and 2 μL Nafion solution (2 wt%) were added on the surface of dry glassy carbon electrode and dried at room temperature. The serum containing different concentrations of DA was used as electrolyte.. DPV measurements of DA detection were carried out in the potential range of -0.6-0.2V, and the amplitude, pulse width and pulse period were set to 50 mV, 0.05 s and 0.25 s, respectively.

3. Results and discussion

3.1. Characterization of N-GDQDs

The morphology of the prepared N-GDQDs is characterized by TEM and AFM. It can be seen that N-GDQDs are almost uniformly dispersed and spherical with an

average diameter of 5.2±2 nm (Fig. 1a). Fig. 1b shows the HRTEM image of N-GDQDs, which clearly reveals the good crystallinity of N-GDQDs with a lattice spacing of 0.37 nm, which is basically consistent with the lattice spacing of GDY [27]. It can be seen from the AFM image that the typical topographic height of N-GDQDs is in the range of 4-6 nm (Fig. 1c). The composition of the prepared N-GDQDs is characterized by Raman spectroscopy and X-ray photoelectron spectroscopy (XPS). Fig. 1d shows that the peaks at 1384 and 1589 cm^{-1} correspond to the D band and G band of N-GDQDs, respectively. The I_D/I_G values are 0.632, 0.775 and 0.824, respectively. The increased I_D/I_G value indicates more defects in N-GDQDs are caused by N-doping [28]. The two weak peaks at 1922 and 2186 cm^{-1} are attributed to the vibration of the conjugated diyne bond (−C≡C−C≡C−), which is consistent with previous reports [29]. It's proved that N-GDQDs still have a carbon skeleton similar to that of GDY and GDQDs after the introduction of nitrogen. XPS spectrum shows GDY and GDQDs mainly contain carbon and oxygen elements, and N speak appears after N doping (Fig. S1). In the XPS of N-GDQDs, there are three peaks at 282.1, 398.2 and 529.2 eV, corresponding to C1s, N1s and O1s, respectively. The C1s peak of N-GDQDs (Fig. 1e) can be proposed to be merged into four bonds: C–C (sp^2) at 284.4 eV, C–C (sp) at 284.9 eV, C=N/C=O at 286 eV and C–O at 288.5 eV [28]. N 1s spectrum (Fig. 1f) can be deconvoluted into the pyrrole N (C–N–C, 397.7 eV) and graphite N ($N–(C)_3$, 399.6 eV), which indicate that N atoms have successfully doped into the carbon skeleton of N-GDQDs [30]. The pyrrole N (C–N–C) is formed through substituting the carbon atoms in-between diyne linkages (−C≡C−C≡C−) groups by N atoms [31]. The above analysis and demonstration are consistent with the results of FT-IR (Fig. S2).

<Fig. 1>

3.2. Optical properties of N-GDQDs

Fig. 2a shows the absorption band of N-GDQDs decreases from 300 nm to 800 nm, and an insignificant absorption band at ca. 320 nm is observed, which is attributed to n-π* transitions of conjugated domains of N-GDQDs [32]. GDQDs and N-GDQDs have similar UV-vis absorption band (Fig. S3). The doping of heteroatoms can change the optical properties of carbon based quantum dots and improve their quantum yield

[33]. In our previous work, the quantum yield of the prepared GDQDs is 14.6% [26]. The quantum yield of N-GDQDs is 48.6%, which reveals the introduction of nitrogen greatly improves the optical properties of N-GDQDs. The comparison of fluorescence photos before and after N doping is shown in Fig. S4, which is consistent with the result. Fig. 2b shows the maximum and the best excitation and emission absorption spectra of N-GDQDs. The optimal excitation and emission wavelengths are determined to be 319 nm and 410 nm, respectively. The conclusion is further confirmed by 3D images drawn and scanned at different excitation wavelengths (x axis: 260-340 nm) and emission wavelengths (y axis: 350-550 nm) (Fig. 2c). In addition, the emission spectra at different excitation wavelengths are studied as shown in Fig. 2d (279-359 nm). With the increase of excitation wavelength, the emission peak is gradually red-shifted. It is due to the different band gaps of different sizes of N-GDQDs and the existence of different emission traps or different surface defect states [34]. Fig. 2e and f show the fluorescence changes little after existing in different concentrations of salt solution or continuous UV irradiation for 7000 s, which shows that N-GDQDs have good tolerance to high salt and photobleaching.

<Fig. 2>

3.3. Electrochemical properties of N-GDQDs

The electrocatalytic performance of the modified electrode is studied at a scanning rate of 100 mV s^{-1}. Fig. 3a shows the peak current of N-GDQDs is higher than that of other modified electrodes because of its large carbon pores and the introduction of nitrogen [35]. And the ΔEp potential difference of N-GDQDs is the smallest, which indicates that it has stronger electrocatalytic oxidation ability than GDY and GDQDs. The electrocatalytic behavior of surface-modified electrodes is investigated through EIS (Fig. 3b). A smaller semicircle with an electron transfer resistance (Rct) value of 424 Ω for N-GDQDs modified GCE than those of GDQDs (515 Ω), GDY (678 Ω) is observed. It shows that N-GDQDs have lower resistance, and it is easier for electrons to transfer to the surface of the modified electrode. Fig. 3c displays the CV of bare GCE, GDY, GDQDs and N-GDQDs modified GCE electrode in PBS buffer containing 100 μM DA. The bare GCE, GDY/GCE and GDQDs/GCE exhibit weak electrocatalytic

ability evident from the observed feeble oxidation peaks at relatively higher over potentials. On the contrary, N-GDQDs/GCE delivers a large peak current originated from the electrocatalytic oxidation for DA. In order to realize the reaction mechanism and dynamic parameters of N-GDQDs/GCE electrode, the effect of scanning rate on the peak current and potential of DA is investigated. The oxidation peaks current intensity (C_i) increases gradually with the increase of scan rate (ν) (Fig. 3d). The C_i is proportional to the square root of the scanning rate (R^2=0.99), suggesting the oxidation of DA is controlled by diffusion process [36].

<Fig. 3>

3.4. Analytical performance of the sensor

The experimental conditions for electrochemical detection of DA including the pH value of the assay and the amount of electrode dripping are optimized, N-GDQDs shows the highest current intensity at pH=7.0 and 6 μL dripping quantitative amounts (Fig. S5). Under the optimized conditions, the sensitivity of DA electrochemical detection is investigated. Fig. 4a shows amperometric responses of N-GDQDs modified GCE upon successive addition of DA. With the increase of the concentration of DA, the peak current of N-GDQDs/GCE increases gradually. Clearly, there is a good linear relationship between DA concentration and current in the range of 0.05-240 μM with a correlation coefficient R^2 = 0.98 (Fig. 4b). The LOD is 0.02 μM (S/N = 3).

<Fig. 4>

The experimental conditions for fluorescent detection of DA including the pH value of the assay are investigated and optimized, that the best quenching effect occurs when pH = 6.0 (Fig. S6). Fig. 4c shows the fluorescence spectra of N-GDQDs solution with the addition of different DA concentrations. The fluorescence intensity of N-GDQDs at 410 nm decreases with the increase of DA concentration. The curves of quenching ratio F_0-F and DA concentration from 0 to 600 μM are performed (Fig. 4d), where F_0 and F are the fluorescence intensity of N-GDQDs solution before and after the addition of DA, respectively. The LOD is 0.14 μM (S/N = 3), with a linear range of 0.32-500 μM is obtained (R^2 = 0.99). Similar works are summarized in Table. 1, compared with the other fluorescent and electrochemical sensors, this nanosensor has a wider linear range

and a lower LOD. The normal content of DA in healthy people is in the range of 1.3–2.6 μM [10], which is within the linear range of our detection, which shows a clear potential for real sample measurement.

<Table 1>

3.5. Selectivity, reproducibility and stability.

In order to verify the selectivity of electrochemical method, chronoamperometric measurement is conducted on the N-GDQDs modified GCE under the potential of 0.84 V, followed by injecting 50 μM DA, and 1 mM potential interfering substances (KCl, NaCl, Glycine, L-cystein, Sodium Nitrate, Hydrogen Peroxide, Glucose, Histamine, Glutamic acid) the same solution one by one. As presented in Fig. 5a, excepting a significant current response caused by the addition of DA, the presence of other high-concentration of interfering substances only leads to slight changes in current signal and has negligible influence on current intensity. These results indicate that N-GDQDs/GCE has high selectivity for DA detection. In order to study the reproducibility of the electrode preparation procedure, in the preparation of DA sensor (Fig. 5b), 10 different GCEs with the same modification of 6 μL N-GDQDs are used for the determination of 50 μM DA. The RSD for the between electrode peak currents (average of three determinations on each electrode) is calculated to be 2.8% and the RSD of the currents for 10 replicate measurements on a single electrode in DA is 3.2%. The GCE is polished and dripped with N-GDQDs suspension, and then dried and stored in air for 1 to 5 weeks, and its catalytic activity is measured. As shown in Fig. 5c, after being stored in air for a period of time, the catalytic activity of the DA sensor decreases slightly, and the activity of N-GDQDs still maintains 90% after exposure in air for 2 weeks. The results indicate that the modified electrode has superior stability, high reproducibility and repeatability in both the preparation procedure and the determinations.

<Fig. 5>

The selectivity of the fluorescnce sensor is investigated, and the control experiments are carried out. Firstly, 0.5 mM of DA and 1 mM interfering substances (KCl, NaCl, Glycine, L-cystein, Sodium Nitrate, Hydrogen Peroxide, Glucose, Histamine, Glutamic

acid, and the fluorescence) are added to different N-GDQDs solutions, respectively. The changes of fluorescence intensity in different systems were recorded. The results show that the fluorescence intensity of the system has little change after the addition of other interfering substances, and the fluorescence quenching rate of DA to N-GDQDs sensor is much higher than that of other high-concentration of interfering substances (Fig. 5d), indicating that N-GDQDs has a good selectivity for DA detection.

3.6. The mechanism of the N-GDQDs sensor to DA in optical and electrochemical mode

To understand the possible fluorescence sensing quenching mechanism, the lifetime of fluorescence decay of N-GDQDs without and with different concentrations of DA is investigated. The fluorescence decay time of N-GDQDs is 6.53 ns after the addition of DA (Fig. S7), and the decay time doesn't change obviously when the concentration are 100 μM (6.32 ns) and 200 μM (6.19 ns), which suggests the quenching process belongs to static quenching [49], and a non-fluorescent complex is formed between the fluorescent substance and the quenchant [51]. To test this hypothesis, homologous substances of DA (β-phenethylamine, tyramine, catechol, o-benzoquinone and DA-quinone) are selected to study the complexation state between N-GDQDs and DA (Fig. 6a). Fig. 6a shows the fluorescence of N-GDQDs isn't quenched after adding β-phenethylamine, o-benzoquinone, DA-quinone and tyramine. On the contrary, the fluorescence is quenched after adding catechol and DA. Both catechol and DA share the same group, i.e. catechol group. We infer that the catechol group is the source of fluorescence quenching of N-GDQDs [49]. To confirm this, DA-quinone and o-benzoquinone (oxidized by H_2O_2) are used to investigate the quenching effect by N-GDQDs, and both of them show no quenching effect. Thus, catechol group in DA plays the key role for quenching effect. Phenoxy anions (in PBS solution) in DA show big affinity to pyridinic N sites of N-GDQDs, due to their donor-bridge-acceptor structure, forming a ground-state non-fluorescent complex [49]. The above results indicate catechol group in DA plays a key role in fluorescent detection of DA， that N-GDQDs fluorescent detection method has good specificity.

<Fig. 6>

The mechanism of electrochemical detection of DA by N-GDQDs/GCE (Fig. 6b)

is investigated. The oxidation reaction of N-GDQDs toward DA is strongly related to the pyridinic N structure in N-GDQDs and the catechol group in DA. DA can be oxidized to DA-benzodiquinone under electric field through N-GDQDs/GCE, and forms a complex between N-GDQDs and DA-benzodiquinone [50]. Due to the specific donor-bridge-acceptor structures with a large conjugated domain, the phenoxy anion of DA is easily adsorbed on the surface of N-GDQDs, pyridinic N is the preferred position. Large delocalized π conjugated structures connect N-GDQDs to DA molecules to form complex DA products. Furthermore, this complex excludes the other interferences, resulting in a better selectivity.

3.7. Real application of N-GDQDs for analysis of DA in human serum samples

Through the actual recovery detection of DA in human serum samples, the biological application potential of N-GDQDS solution in actual samples is explored. Firstly, the detection of DA in human serum by N-GDQDs/GCE under electrochemical detection method is explored, as shown in Table. 2. The ratio of DA detection to addition in human serum samples ranges from 98.89% to 102.50%, and RSD ranges from 2.22% to 3.33%. The deviation between the electrochemical detection results of N-GDQDs/GCE and the actual amount of DA is small, indicating that this method has good practical application in the detection of DA in actual samples, and the detection results are relatively reliable.

In the fluorescence detection of DA in actual samples based on N-GDQDS solution, the addition detection experiment of human serum samples is also carried out to evaluate the feasibility. Three different concentrations of DA are added to the sample solution. As shown in Table. 2, the recovery range of relevant samples is 97.93-107.03%. The relative standard deviation (n=3) is between 2.74% and 3.70%. The high recovery rate and standard deviation indicate the reliability of N-GDQDs solution for the fluorescence detection of DA in practical samples, which proves that the method has great application potential in the clinical detection of DA.

<Table 2>

4. Conclusions

N-GDQDs are successfully prepared from urea and GDY powder by ultrasonic crushing and hydrothermal method. The introduction of nitrogen greatly improves the fluorescence performance with the quantum yield enhanced from 14.6% to 48.6%, and facilitates electron transferring of N-GDQDs due to improved conductivity. A novel electrochemical and fluorescence detection mechanism is designed for DA detection. In the electrochemical detection, the linear range is 0.05-240 μM and the LOD is 0.02 μM. The LOD of DA by fluorescence method is 0.14 μM, and the linear range is 0.32-500 μM. Either mode shows a similar level for DA detection, but the sensor significantly improves the accuracy and reliability of detection. In addition, the selective exploration of detection and the recovery experiment in actual serum samples show that this method has a clear potential for the real-sampled detection.

Declaration of Competing Interest

The authors declare no conflicts of interest.

Acknowledgements

This work was supported by the National Natural Science Foundation of China (Grant No. 21501106, 31800800), Natural Science Foundation of Shandong Province (Grant No. ZR2020MB026, ZR202103010467), and Qingdao Municipal Science and Technology Commission (Grant No. 19-6-2-73-cg, 16-5-1-86-jch).

References

[1] V.M. Krishna, T. Somanathan, E. Manikandan, K.K. Tadi, S. Uvarajan, Neurotransmitter Dopamine Enhanced Sensing Detection Using Fibre-Like Carbon Nanotubes by Chemical Vapor Deposition Technique, J. Nanosci. Nanotechno. 18(8) (2018) 5380-5389.

[2] X. Lin, Y. Zhang, W. Chen, P. Wu, Electrocatalytic oxidation and determination of dopamine in the presence of ascorbic acid and uric acid at a poly (p-nitrobenzenazo resorcinol) modified glassy carbon electrode, Sens. Actuator B-Chem. 122(1) (2007) 309-314.

[3] X. Liu, J. Liu, Biosensors and sensors for dopamine detection, View (2020).

[4] Y. Suzuki, Development of Fluorescent Reagent Based on Ligand Exchange Reaction for the Highly Sensitive and Selective Detection of Dopamine in the Serum, Sensors-Basel 19(18) (2019) 3928-.

[5] T.C. Napier, A. Kirby, A.L. Persons, The role of dopamine pharmacotherapy and addiction-like behaviors in Parkinson's disease, Prog. Neuro-Psychoph. 102 (2020).

[6] M.J. Berridge, Dysregulation of neural calcium signaling in Alzheimer disease,

bipolar disorder and schizophrenia, Prion 7(1) (2013) 2-13.
[7] X.F. Pan, A.C. Kaminga, S.W. Wen, X.Y. Wu, K. Acheampong, A.Z. Liu, Dopamine and Dopamine Receptors in Alzheimer's Disease: A Systematic Review and Network Meta-Analysis, Front Aging Neurosci. 11 (2019).
[8] A.E. Whitton, J.M. Reinen, M. Slifstein, Y.S. Ang, P.J. McGrath, D.V. Iosifescu, A. Abi-Dargham, D.A. Pizzagalli, F.R. Schneier, Baseline reward processing and ventrostriatal dopamine function are associated with pramipexole response in depression, Brain 143(2) (2020) 701-710.
[9] P. Balasubramanian, T.S.T. Balamurugan, S.-M. Chen, T.-W. Chen, T. Sathesh, Rational Design of Cu@Cu_2O Nanospheres Anchored B, N Co-doped Mesoporous Carbon: A Sustainable Electrocatalyst To Assay Eminent Neurotransmitters Acetylcholine and Dopamine, ACS Sustain. Chem. Eng. 7(6) (2018) 5669-5680.
[10] Z. Chen, C. Zhang, T. Zhou, H. Ma, Gold nanoparticle based colorimetric probe for dopamine detection based on the interaction between dopamine and melamine, Microchim. Acta 182(5-6) (2014) 1003-1008.
[11] Z. Jiang, P. Gao, L. Yang, C. Huang, Y. Li, Facile in Situ Synthesis of Silver Nanoparticles on the Surface of Metal–Organic Framework for Ultrasensitive Surface-Enhanced Raman Scattering Detection of Dopamine, Anal. Chem. 87(24) (2015) 12177-12182.
[12] Q.T. Huang, X.F. Lin, L.L. Tong, Q.X. Tong, Graphene Quantum Dots/Multiwalled Carbon Nanotubes Composite-Based Electrochemical Sensor for Detecting Dopamine Release from Living Cells, ACS Sustain. Chem. Eng. 8(3) (2020) 1644-.
[13] Y. Xue, B. Huang, Y. Yi, Y. Guo, Z. Zuo, Y. Li, Z. Jia, H. Liu, Y. Li, Anchoring zero valence single atoms of nickel and iron on graphdiyne for hydrogen evolution, Nat. Commun. 9(1) (2018) 1460.
[14] Q.T. Huang, X.F. Lin, J.J. Zhu, Q.X. Tong, Pd-Au@carbon dots nanocomposite: Facile synthesis and application as an ultrasensitive electrochemical biosensor for determination of colitoxin DNA in human serum, Biosens. Bioelectron. 94 (2017) 507-512.
[15] P. Chaturvedi, S. Sarker, X.Q. Chen, S. Das, H.M. Luo, S.N. Smirnov, Enhancing the Cooperative Catalytic Effect in Ni/Co Hydr(oxy)oxide Porous Electrodes for Overall Water Splitting and Glucose Sensing, ACS Sustain. Chem. Eng. 7(13) (2019) 11303-11312.
[16] S. Mondal, C. Subramaniam, Point-of-Care, Cable-Type Electrochemical Zn2+ Sensor with Ultrahigh Sensitivity and Wide Detection Range for Soil and Sweat Analysis, ACS Sustain. Chem. Eng. 7(17) (2019) 14569-14579.
[17] P. Ni, C. Chen, Y. Jiang, C. Zhang, B. Wang, Y. Lu, H. Wang, A fluorescent assay for alkaline phosphatase activity based on inner filter effect by in-situ formation of fluorescent azamonardine, Sensor. Actuat. B-Chem. 302 (2020) 127145.
[18] C. Chen, D. Zhao, B. Wang, P. Ni, Y. Jiang, C. Zhang, F. Yang, Y. Lu, J. Sun, Alkaline Phosphatase-Triggered in Situ Formation of Silicon-Containing Nanoparticles for a Fluorometric and Colorimetric Dual-Channel Immunoassay, Anal. Chem. 92(6) (2020) 4639-4646.

[19] X.Q. Chen, N. Zheng, S.F. Chen, Q. Ma, Fluorescence detection of dopamine based on nitrogen-doped graphene quantum dots and visible paper-based test strips, Anal. Methods-UK 9(15) (2017) 2246-2251.
[20] Y.B. Liu, X. He, P.Y. Ma, Y.B. Huang, X.L. Li, Y. Sun, X.H. Wang, D.Q. Song, Fluorometric detection of dopamine based on 3-aminophenylboronic acid-functionalized AgInZnS QDs and cells imaging, Talanta 217 (2020).
[21] H. Min, Y.Q. Qi, Y.H. Chen, Y.L. Zhang, X.X. Han, Y. Xu, Y. Liu, J.S. Hu, H.B. Liu, Y.Y. Li, G.J. Nie, Synthesis and Imaging of Biocompatible Graphdiyne Quantum Dots, ACS Appl. Mater. Inter. 11(36) (2019) 32798-32807.
[22] S. Du, Y. Wang, Z. Liu, Z. Xu, H. Zhang, A portable immune-thermometer assay based on the photothermal effect of graphene oxides for the rapid detection of Salmonella typhimurium, Biosens. Bioelectron. 144 (2019) 111670.
[23] Y.S. Zhao, H.J. Tang, N.L. Yang, D. Wang, Graphdiyne: Recent Achievements in Photo- and Electrochemical Conversion, Adv. Sci. 5(12) (2018).
[24] Y.S. Zhao, J.W. Wan, H.Y. Yao, L.J. Zhang, K.F. Lin, L. Wang, N.L. Yang, D.B. Liu, L. Song, J. Zhu, L. Gu, L. Liu, H.J. Zhao, Y.L. Li, D. Wang, Few-layer graphdiyne doped with sp-hybridized nitrogen atoms at acetylenic sites for oxygen reduction electrocatalysis, Nat. Chem. 10(9) (2018) 924-931.
[25] A. Karimzadeh, M. Hasanzadeh, N. Shadjou, M. de la Guardia, Optical bio(sensing) using nitrogen doped graphene quantum dots: Recent advances and future challenges, Trac-Trend. Anal. Chem. 108 (2018) 110-121.
[26] Q. Bai, C.Y. Zhang, L. Li, Z.L. Zhu, L.N. Wang, F.Y. Jiang, M.H. Liu, Z.B. Wang, W.W. Yu, F.L. Du, Z.G. Yang, N. Sui, Subsequent monitoring of ferric ion and ascorbic acid using graphdiyne quantum dots-based optical sensors, Microchim. Acta 187(12) (2020).
[27] P.Y. Kuang, B.C. Zhu, Y.L. Li, H.B. Liu, J.G. Yu, K. Fan, Graphdiyne: a superior carbon additive to boost the activity of water oxidation catalysts, Nanoscale Horiz. 3(3) (2018) 317-326.
[28] S.L. Zhang, H.P. Du, J.J. He, C.S. Huang, H.B. Liu, G.L. Cui, Y.L. Li, Nitrogen-Doped Graphdiyne Applied for Lithium-Ion Storage, ACS Appl. Mater. Inter. 8(13) (2016) 8467-8473.
[29] S.Y. Guo, H.L. Yan, F. Wu, L.J. Zhao, P. Yu, H.B. Liu, Y.L. Li, L.Q. Mao, Graphdiyne as Electrode Material: Tuning Electronic State and Surface Chemistry for Improved Electrode Reactivity, Anal. Chem. 89(23) (2017) 13008-13015.
[30] Z.Y. Yan, X.C. Qu, Q.Q. Niu, C.Q. Tian, C.J. Fan, B.F. Ye, A green synthesis of highly fluorescent nitrogen-doped graphene quantum dots for the highly sensitive and selective detection of mercury(II) ions and biothiols, Anal. Methods-UK 8(7) (2016) 1565-1571.
[31] R. Pietrzak, XPS study and physico-chemical properties of nitrogen-enriched microporous activated carbon from high volatile bituminous coal, Fuel 88(10) (2009) 1871-1877.
[32] G.N. Kalantzopoulos, F. Lundvall, S. Checchia, A. Lind, D.S. Wragg, H. Fjellvag, B. Arstad, In Situ Flow MAS NMR Spectroscopy and Synchrotron PDF Analyses of the Local Response of the BrOnsted Acidic Site in SAPO-34 during Hydration at

Elevated Temperatures, Chemphyschem 19(4) (2018) 519-528.
[33] J.J. Niu, H. Gao, Synthesis and drug detection performance of nitrogen-doped carbon dots, J. Lumin. 149 (2014) 159-162.
[34] J. Peng, W. Gao, B.K. Gupta, Z. Liu, R. Romero-Aburto, L.H. Ge, L. Song, L.B. Alemany, X.B. Zhan, G.H. Gao, S.A. Vithayathil, B.A. Kaipparettu, A.A. Marti, T. Hayashi, J.J. Zhu, P.M. Ajayan, Graphene Quantum Dots Derived from Carbon Fibers, Nano Lett. 12(2) (2012) 844-849.
[35] A. Ramachandran, A.N. J S, S. Karunakaran Yesodha, Polyaniline-Derived Nitrogen-Doped Graphene Quantum Dots for the Ultratrace Level Electrochemical Detection of Trinitrophenol and the Effective Differentiation of Nitroaromatics: Structure Matters, ACS Sustain. Chem. Eng. 7(7) (2019) 6732-6743.
[36] J.F. Guan, J. Zou, Y.P. Liu, X.Y. Jiang, J.G. Yu, Hybrid carbon nanotubes modified glassy carbon electrode for selective, sensitive and simultaneous detection of dopamine and uric acid, Ecotox. Environ. Safe. 201 (2020).
[37] J. Tang, S. Jiang, Y. Liu, S. Zheng, L. Bai, J. Guo, J. Wang, Electrochemical determination of dopamine and uric acid using a glassy carbon electrode modified with a composite consisting of a Co(II)-based metalorganic framework (ZIF-67) and graphene oxide, Microchim. Acta 185(10) (2018) 486.
[38] J. Xiao, H. Wang, C. Li, K. Deng, X. Li, A simple dopamine sensor using graphdiyne nanotubes and shortened carbon nanotubes for enhanced preconcentration and electron transfer, Microchem. J. 160 (2021) 105755.
[39] D.C. Poudyal, A.K. Satpati, S. Kumar, S.K. Haram, High sensitive determination of dopamine through catalytic oxidation and preconcentration over gold-multiwall carbon nanotubes composite modified electrode, Mater. Sci. Eng. C 103 (2019) 109788.
[40] X. Guo, H. Yue, S. Song, S. Huang, X. Gao, H. Chen, P. Wu, T. Zhang, Z. Wang, Simultaneous electrochemical determination of dopamine and uric acid based on MoS2nanoflowers-graphene/ITO electrode, Microchem. J. 154 (2020) 104527.
[41] K. Zhou, D. Shen, X. Li, Y. Chen, L. Hou, Y. Zhang, J. Sha, Molybdenum oxide-based metal-organic framework/polypyrrole nanocomposites for enhancing electrochemical detection of dopamine, Talanta 209 (2020) 120507.
[42] X. Zhang, L. Zhang, W.-W. Ma, Y. Zhou, Z.-N. Lu, S. Xu, A Near-Infrared Ratiometric Fluorescent Probe for Highly Selective Recognition and Bioimaging of Cysteine, Front. Chem. 7(32) (2019).
[43] H. Wang, H. Rao, M. Luo, X. Xue, Z. Xue, X. Lu, Noble metal nanoparticles growth-based colorimetric strategies: From monocolorimetric to multicolorimetric sensors, Coordin. Chem. Rev. 398 (2019) 113003.
[44] X. Xu, D. Ren, Y. Chai, X. Cheng, J. Mei, J. Bao, F. Wei, G. Xu, Q. Hu, Y. Cen, Dual-emission carbon dots-based fluorescent probe for ratiometric sensing of Fe(III) and pyrophosphate in biological samples, Sensor. Actuat. B-Chem 298 (2019) 126829.
[45] Y. Gao, X. Yan, M. Li, H. Gao, J. Sun, S. Zhu, S. Han, L.-N. Jia, X.-E. Zhao, H. Wang, A “turn-on” fluorescence sensor for ascorbic acid based on graphene quantum dots via fluorescence resonance energy transfer, Anal. Methods-UK 10(6) (2018) 611-616.
[46] X. Guo, G. Yue, J. Huang, C. Liu, Q. Zeng, L. Wang, Label-Free Simultaneous

Analysis of Fe(III) and Ascorbic Acid Using Fluorescence Switching of Ultrathin Graphitic Carbon Nitride Nanosheets, ACS Appl. Mater. Inter. 10(31) (2018) 26118-26127.
[47] J. Zhao, L. Zhao, C. Lan, S. Zhao, Graphene quantum dots as effective probes for label-free fluorescence detection of dopamine, Sensor. Actuat. B-Chem. 223 (2016) 246-251.
[48] Y. Li, Y. Jiang, T. Mo, H. Zhou, Y. Li, S. Li, Highly selective dopamine sensor based on graphene quantum dots self-assembled monolayers modified electrode, Electroanal. Chem. 767 (2016) 84-90.
[49] Y. Ma, A.Y. Chen, X.F. Xie, X.Y. Wang, D. Wang, P. Wang, H.J. Li, J.H. Yang, Y. Li, Doping effect and fluorescence quenching mechanism of N-doped graphene quantum dots in the detection of dopamine, Talanta 196 (2019) 563-571.
[50] J. Wang, C. Lu, T. Chen, L. Hu, Y. Du, Y. Yao, M.C. Goh, Simply synthesized nitrogen-doped graphene quantum dot (NGQD)-modified electrode for the ultrasensitive photoelectrochemical detection of dopamine, Nanophotonics-Berlin 9(12) (2019) 3831-3839.
[51] X.C. Sun, Y. Wang, Y. Lei, Fluorescence based explosive detection: from mechanisms to sensory materials, Chem. Soc. Rev. 44(22) (2015) 8019-8061.

Table. 1. Comparison of different methods for DA detection.

materials	methods	LOD (nM)	Linear range (μM)	Ref
GO-ZIF67	electrochemical	50	0.2-80	[37]
S-MWCNTs-GDY	electrochemical	8.6	0.02-20	[38]
MWCNTs/AuNPs	electrochemical	35	0.1-10	[39]
MoS_2NFs-rGO/ITO	electrochemical	120	5-60	[40]
CuTRZMoO_4/PPy	electrochemical	80	1-100	[41]
HBT-Cys	fluorescent	500	1-40	[42]
NH_2-CQDs/ AuNCs	fluorescent	500	2-60	[43]
b-CDs	fluorescent	280	1-60	[44]
GQDs	fluorescent	200	1-95	[45]
g-C_3N_4 NNs	fluorescent	180	0.5-30	[46]
GQDs	fluorescent	90	0.25-50	[47]
GQDs	electrochemical	115	1-150	[48]
N-doped GQDs	fluorescent	3.3	0.01-3	[49]
		611	3-7	
N-doped GQDs	electrochemical	30	0.03-450	[50]
			450-9680	
N-GDQDs	electrochemical	22	0.05-240	This work
	fluorescent	140	0.32-500	

Table. 2. Electrochemical and fluorescent recoveries of DA in human serum samples (n=3)

method	Serum sample	Added DA (μM)	Found DA (μM)	Current(μA) / $F-F_0$	Recovery (%)	RSD (%)
electrochemical	1	0	0	-	-	-
	2	1	1.03	16.63	102.50	3.33
	3	5	5.04	17.33	100.71	2.53
	4	20	19.78	20.99	98.89	2.22
fluorescent	1	0	0	-	-	-
	2	1	1.06	6.77	107.03	3.70
	3	5	5.16	33.71	103.20	2.87
	4	20	19.59	121.51	97.93	2.74

Human serum samples was obtained from Qingdao Central Hospital.

Scheme. 1. Synthesis of N-GDQDs and electrochemical and fluorescence detection of DA.

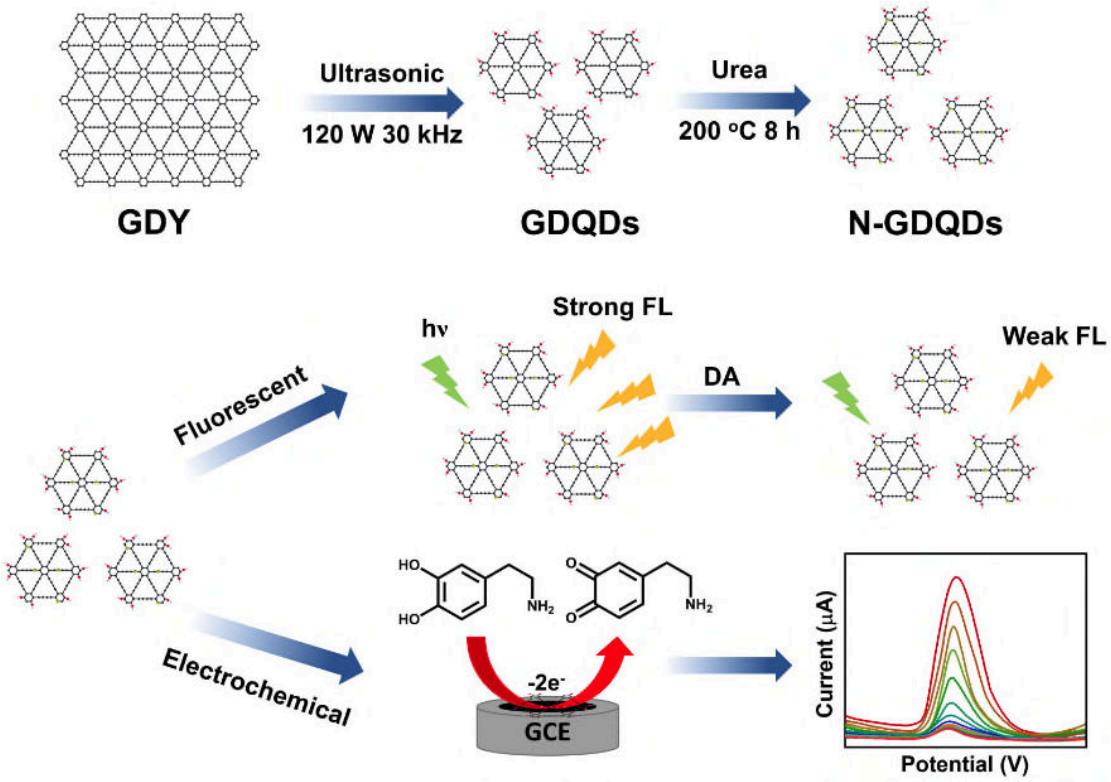


Fig. 1. characterization of N-GDQDs, (a) Representative TEM image of N-GDQDs. Inset: size distribution of N-GDQDs. (b) High-resolution TEM image of N-GDQDs. (c) AFM image of N-GDQDs. (d) Raman spectroscopy of GDY, GDQDs and N-GDQDs. (e) C1s spectra of N-GDQDs. (f) N1s spectra of N-GDQDs.

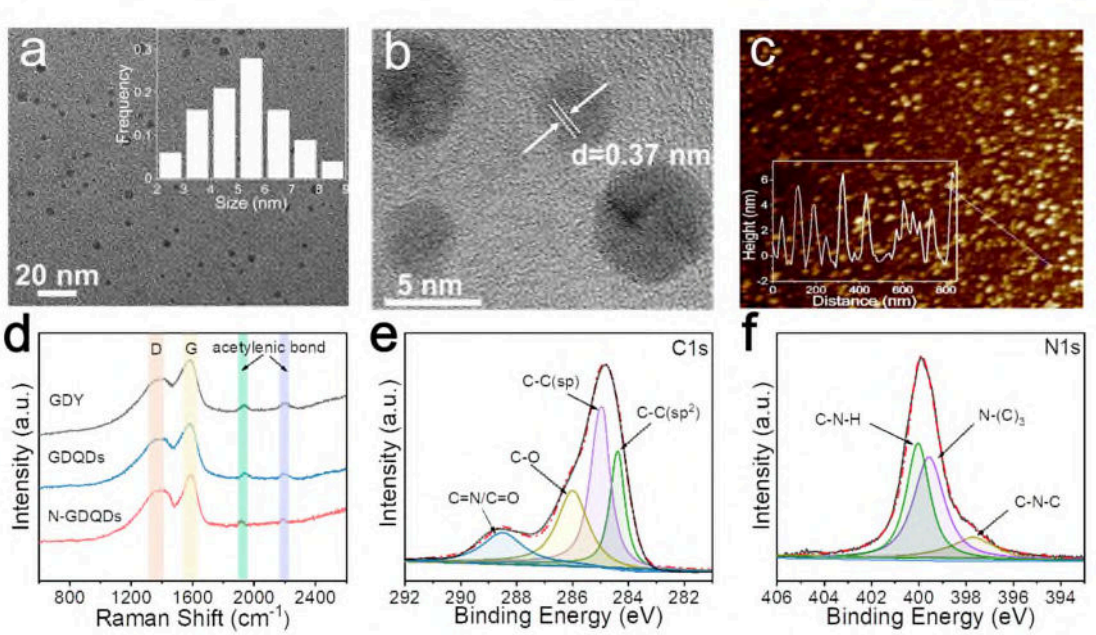


Fig. 2. optical properties of N-GDQDs, (a) UV−vis absorption spectra of N-GDQDs, inset: photographs of N-GDQDs solution (dispersed in water) under sunlight (left) and under 365 nm UV irradiation (right). (b) Excitation and emission spectra of N-GDQDs. (c) 3D fluorescence spectra of N-GDQDs. (d) Fluorescence spectra of N-GDQDs excited at different wavelengths. (e) Photo stability of N-GDQDs under irradiation for 7000 s. (f) Fluorescence intensity (at 410 nm) of N-GDQDs influenced by different concentrations of salt solutions. (n=3)

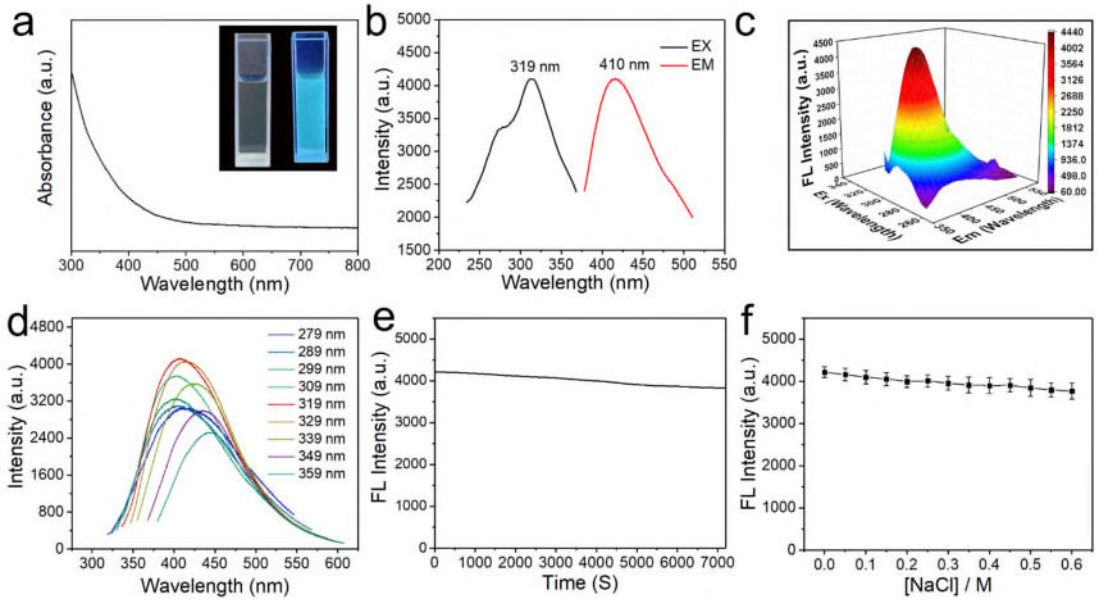


Fig. 3. electrochemical properties of N-GDQDs, (a) Cyclic voltammograms and (b) EIS of the different electrode in the solution of 3 mM $K_3[Fe(CN)_6]$ containing 0.1 M KCl. (c) CV response of the different electrode in 0.1 M PBS (pH=7.0) with the presence of 100 μM of DA; Scan rate: 100 mV s^{-1}. (d) CV curves of N-GDQD/GCE electrode in 0.1 M PBS (pH=7.0) containing 120 μM DA at different scan rates (20-160 mV s^{-1}); inset: the plots of the anodic peak current vs. the square root of scan rate for DA.

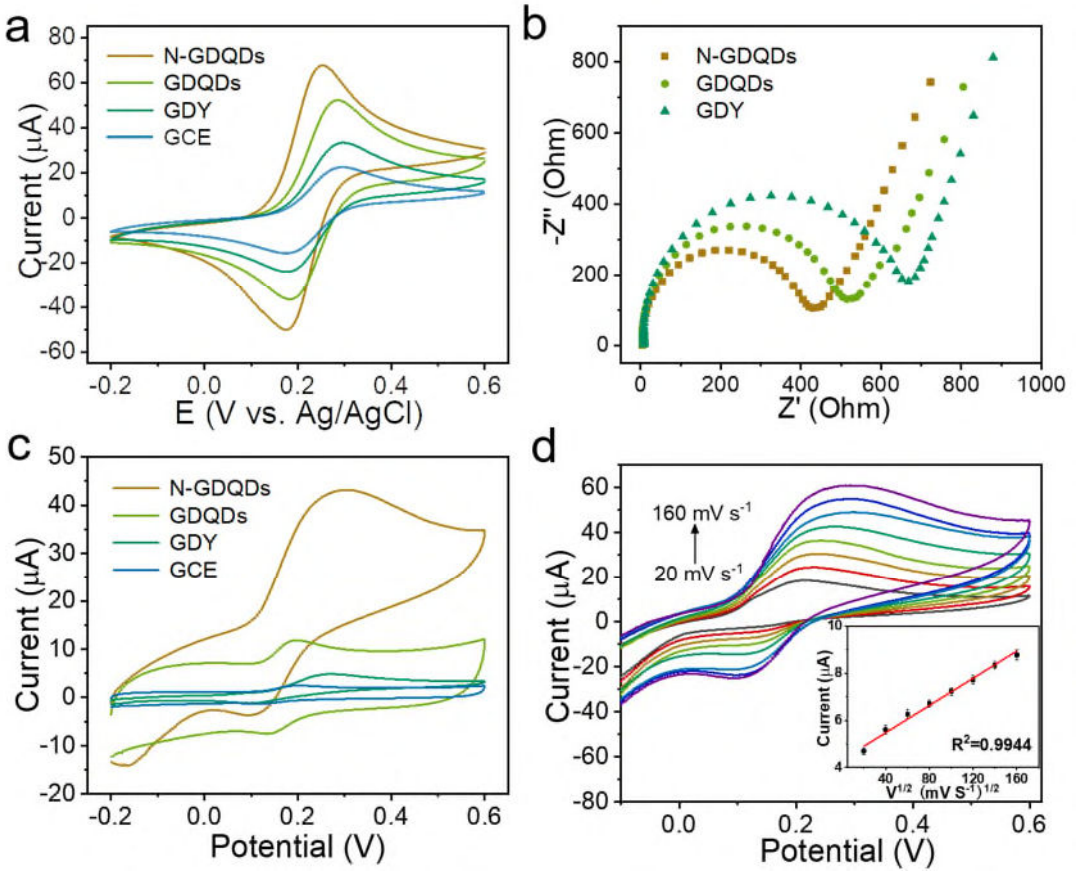


Fig. 4. analytical performance of the sensor, (a) DPV curves of N-GDQDs/GCE in 0.1 M PBS (pH = 7.0) for different concentrations of DA (0-320 μM). (b) The calibration plot of the concentration versus peak current (0.05-240 μM). (c) Fluorescence spectra of N-GDQDs for the detection of different concentrations of DA (from top to bottom: 0-600 μM); (d) Calibration curve of F_0-F versus DA concentration and low concentration DA (0.32-500 μM). (n = 3)

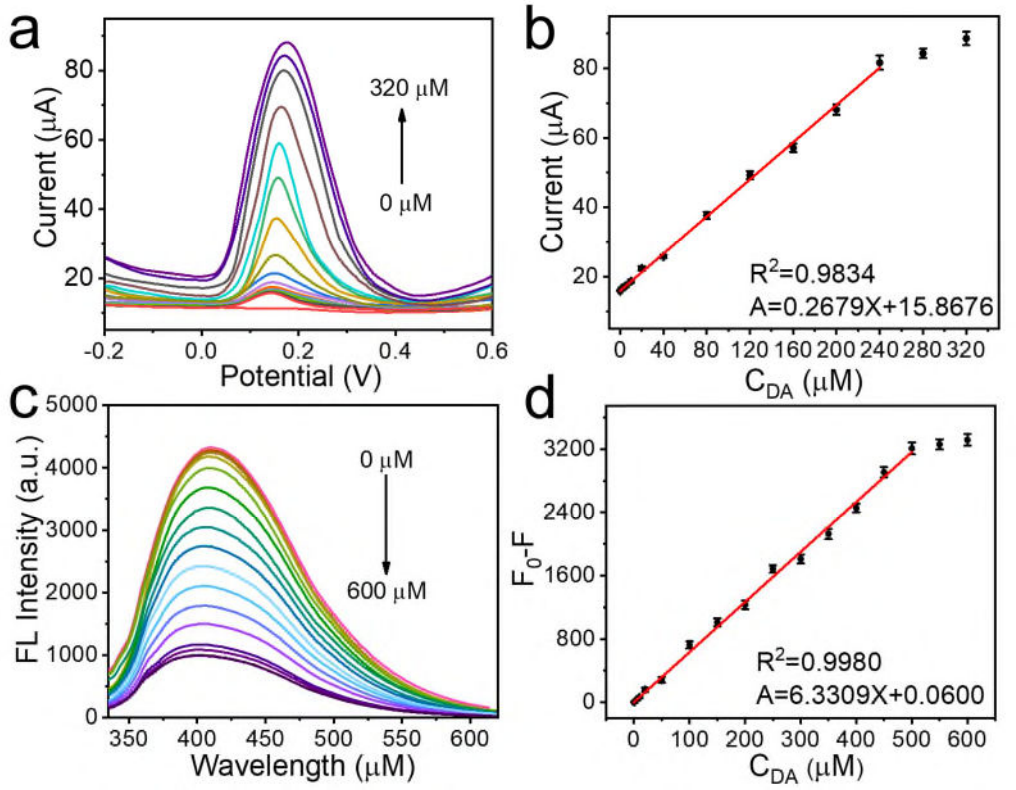


Fig. 5. (a) Electrochemical interference detection of N-GDQDs/GCE after adding different substances. (b, c) Long-term repeatability and stability study of N-GDQDs/GCE for 0.1 mM DA. The error bars represent the standard deviation of three measurements. (d) Fluorescence interference detection of N-GDQDs/GCE after adding different substances. The error bars represent the standard deviation of three measurements. (a: DA, b: KCl, c: NaCl, d: Glycine, e: L-cystein, f: Sodium Nitrate, g: Hydrogen Peroxide, h: Glucose, i: Histamine, j: Glutamic acid)

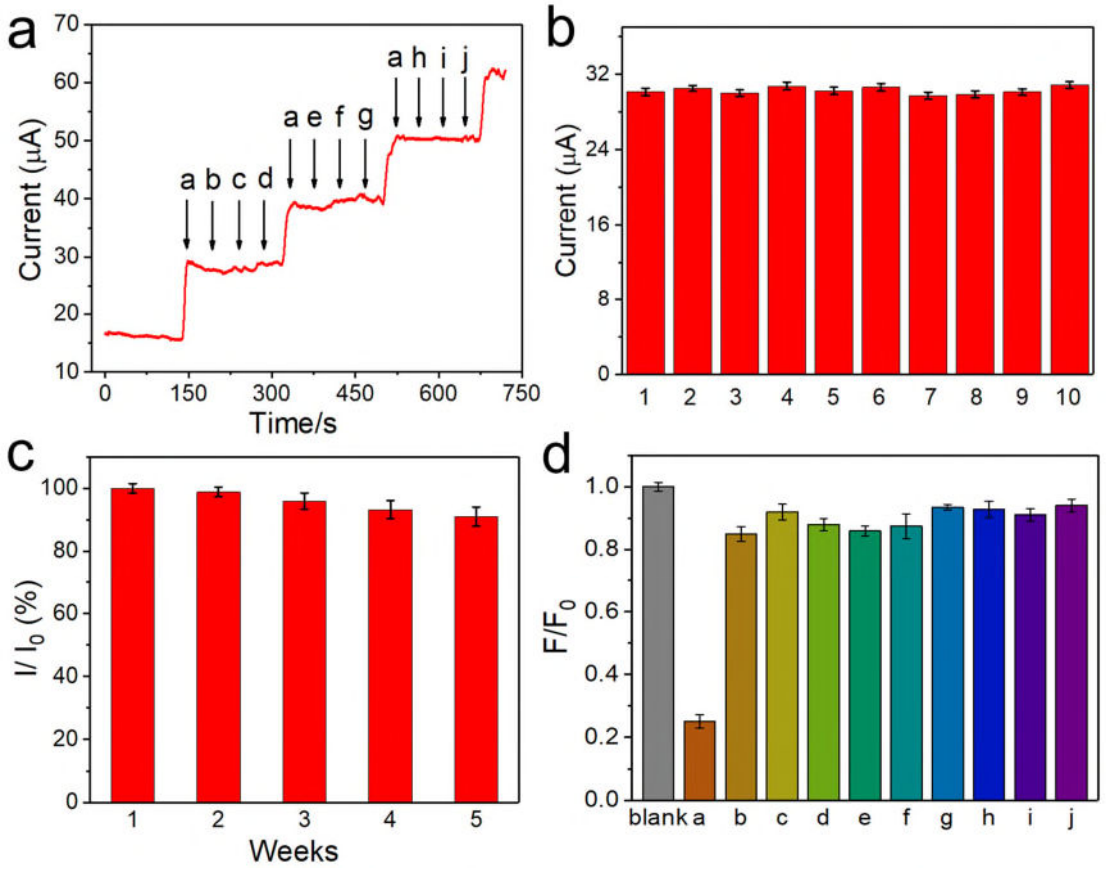
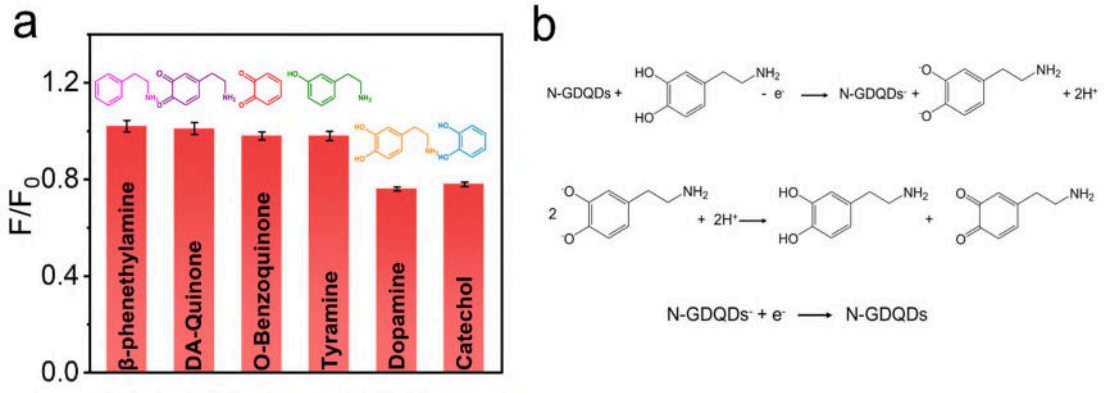


Fig. 6. mechanism of the N-GDQDs sensor to DA, (a) Fluorescence response curves of N-GDQDs after addition of different biomolecules (150 μM). (b) The DA reaction process on N-GDQDs/GCE in Electrochemical detection.



Supplementary Material

Nitrogen-Doped Graphdiyne Quantum-dots as an Optical-Electrochemical Sensor for Sensitive Detection of Dopamine

Qiang Bai[a,1], Hongyang Luo[a,1], Xuetao Yi[b], Shugao Shi[a], Lina Wang[c,*], Manhong Liu[a], Fanglin Du[a], Zhugen Yang[d], Ning Sui[a,*]

[a] College of Materials Science and Engineering, Qingdao University of Science and Technology, Qingdao 266042, China

[b] Qingdao Institute for Food and Drug Control, Qingdao 266000

[c] College of Environment and Safety Engineering, Qingdao University of Science and Technology, Qingdao, 266042, China.

[d] Cranfield Water Science Institute, Cranfield University, Milton Keynes, MK43 0AL, United Kingdom

* Corresponding authors: suining@qust.edu.cn (N. Sui), lnwang2006@163.com (L.N. Wang)

[1] Qiang Bai and Hongyang Luo contributed to this work equally

1. Quantum yields (QYs) measurements

QYs of the N-GDQDs are determined by using quinine sulfate (QY_q=0.560 in water) as the standard sample and are calculated according to the following equation:

$$QY_N = QY_q \frac{I_X}{I_N} \frac{A_N}{A_X} \frac{\eta_X^2}{\eta_N^2}$$

where QY is the quantum yield, the subscript "q" refers to the known QY standard of quinine sulfate, "X" means number of samples, I is the measured integrated emission intensity, A is the ultraviolet absorbance and η is the refractive index.

2.Optimization of the testing conditions

The amount of N-GDQDs on the electrode greatly affects the sensitivity of the sensor. The oxidation peak current increases quickly when the volume of a 0.5 mg mL^{-1} N-GDQDs suspension deposited on the surface of GCE is increased to 6 μL and then levels off (Fig. S5a). This can be related to the increased resistance of the modified electrode to electron transfer and sluggish mass transfer process for DA, which arises from large film thickness of the deposited N-GDQDs suspension on the GCE. Therefore, 6 μL of N-GDQDs suspension is chosen to modify GCE. The influence of solution pH on the electrochemical response of DA at the N-GDQDs modified electrode is examined in PBS (pH 4.0–9.0). As shown in Fig. S5b, the oxidation peak current is greatly influenced by solution pH values. The peak current gradually increases with pH from 4.0 to 7.0. From 7.0 to 9.0, the peak current decreases gradually. Therefore, the optimum pH value of the solution is controlled at 7.0 to carry out the electrochemical

detection of DA. In our daily lives, DA mostly exists in the neutral environment, and N-GDQDs shows the highest catalytic activity at pH=7.0, thus the designed DA sensor has great potential in practical application.

The pH value of the assay for fluorescent detection of DA is investigated and optimized. PBS buffer under different pH value (2.0 to 10.0) is used as a medium for measurement (Fig. S6a). The fluorescence intensity of N-GDQDs reaches the optimum at pH = 6.0. After the addition of DA, sharp decreases of the fluorescence intensity are observed at each pH value (Fig S6b). The largest change of the fluorescence intensity occurs at pH = 6.0 in the absence and presence of DA, which indicates that the best quenching effect occurs when pH = 6.0.

3.Supplementary Figures

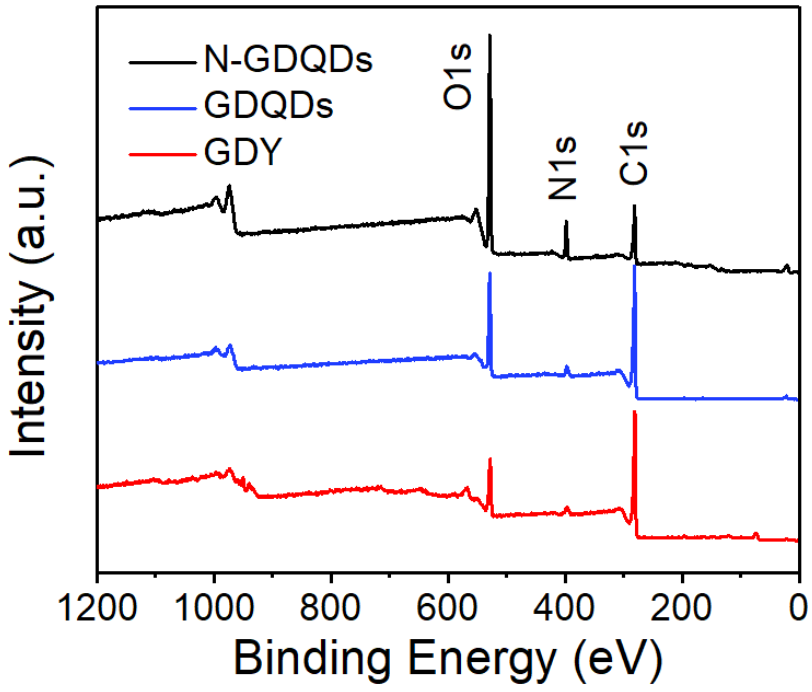


Fig. S1. XPS spectra of GDY, GDQDs and N-GDQDs.

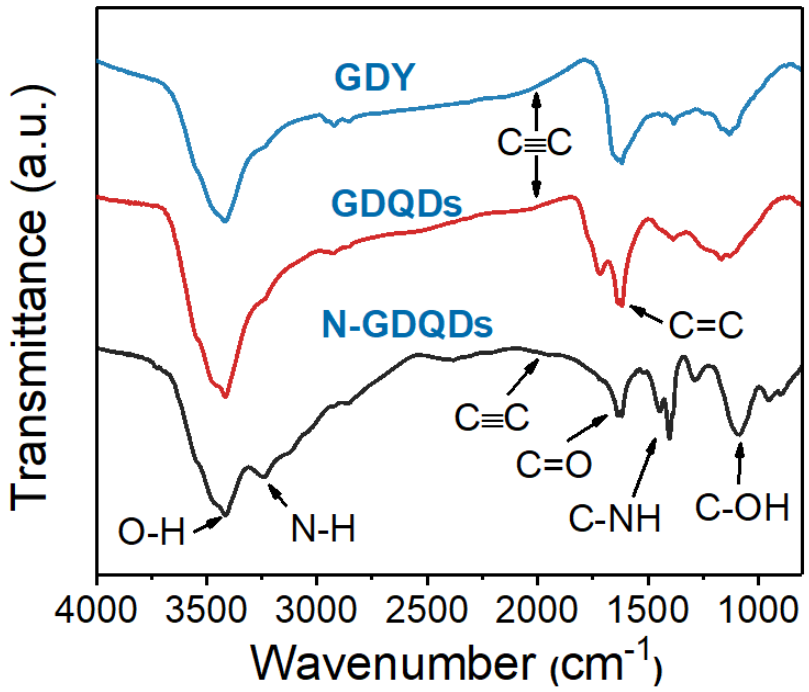


Fig. S2. FT-IR spectra of GDY, GDQDs and N-GDQDs.

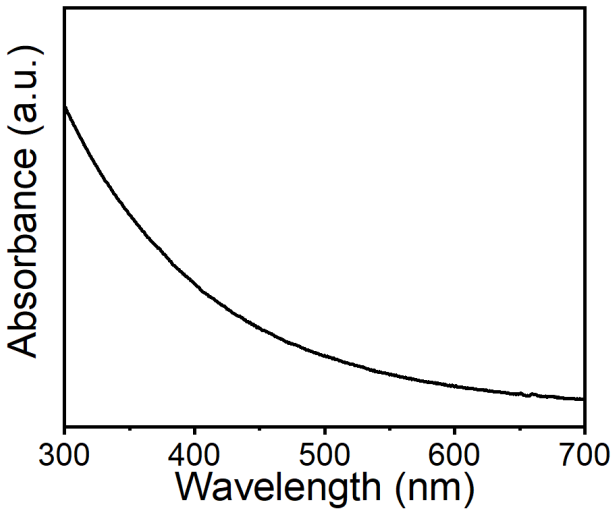


Fig. S3. UV−vis absorption spectra of GDQDs.



Fig. S4. Photographs of N-GDQDs and GDQDs solution dispersed in water under sunlight (1, 3) and under 365 nm UV irradiation (2, 4).

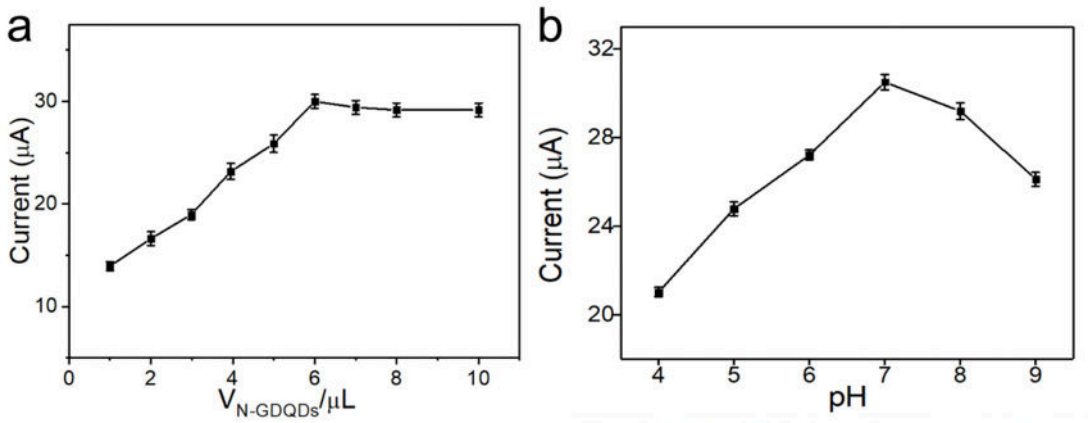


Fig. S5. (a) Current intensity of different dripping amounts to N-GDQDs on GCE. (b) Current intensity of N-GDQDs/GCE under different pH values.

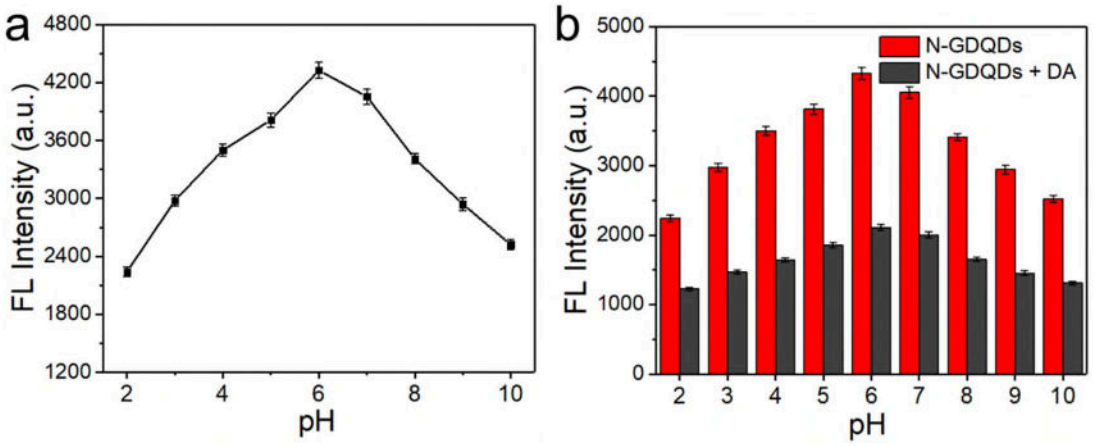


Fig. S6. (a) Fluorescence spectra of N-GDQDs under different pH values. (b) The fluorescence response of N-GDQDs without and with 500 μM DA at different pH values.

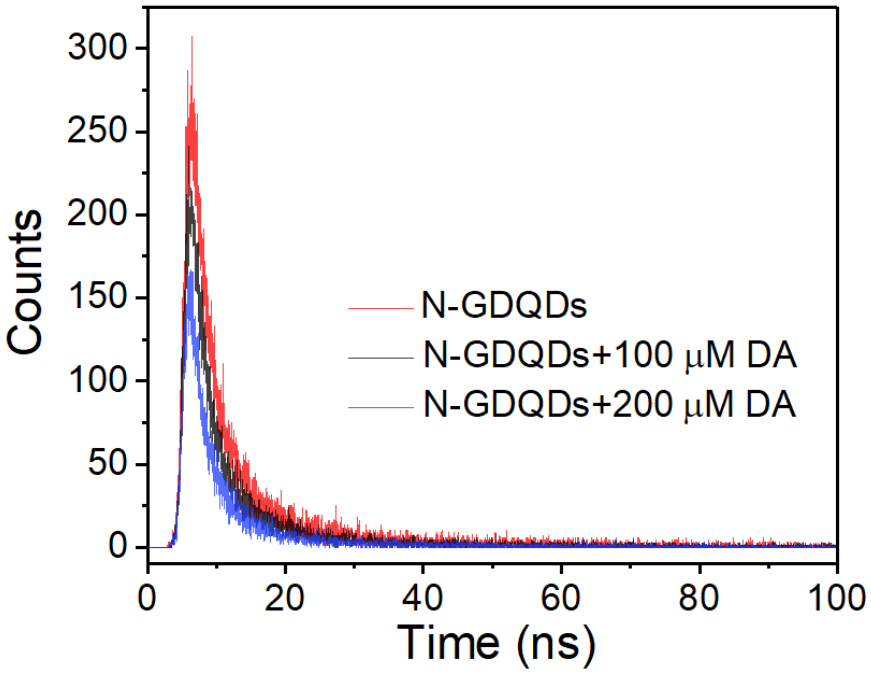


Fig. S7. The fluorescence lifetime of N-GDQDs without DA, with 100 and 200 μM DA.



https://dspace.org/

Nitrogen-doped graphdiyne quantum-dots as an optical-electrochemical sensor for sensitive detection of dopamine

Bai, Qiang; Luo, Hongyang; Yi, Xuetao; Shi, Shugao; Wang, Lina ...

2022-04-22
Elsevier
https://doi.org/10.1016/j.microc.2022.107521
Bai Q, Luo H, Yi X, et al., (2022) Nitrogen-doped graphdiyne quantum-dots as an optical-electrochemical sensor for sensitive detection of dopamine. Microchemical Journal, Volume 179, August 2022, Article number 107521

Downloaded from a DSpace repository. https://dspace.org/